The magnetic propeller accretion regime of LkCa 15

J.-F. Donati, J. Bouvier, S. H. Alencar, C. Hill, A. Carmona, C. P. Folsom, F. Ménard, S. G. Gregory, G. A. Hussain, K. Grankin, et al.

The magnetic propeller accretion regime of LkCa 15

J.-F. Donati,[1]★ J. Bouvier,[2] S. H. Alencar,[3] C. Hill [●],[1] A. Carmona,[1] C. P. Folsom,[1]
F. Ménard,[2] S. G. Gregory,[4] G. A. Hussain,[5] K. Grankin,[6] C. Moutou,[7] L. Malo,[8]
M. Takami,[9] G. J. Herczeg,[10] and the MaTYSSE Collaboration[10]

[1]*Univ. de Toulouse, CNRS, IRAP, 14 avenue Belin, F-31400 Toulouse, France*
[2]*Univ. Grenoble Alpes, CNRS, IPAG, F-38000 Grenoble, France*
[3]*Departamento de Fìsica – ICEx – UFMG, Av. Antônio Carlos, 6627, 30270-901 Belo Horizonte, MG, Brazil*
[4]*SUPA, School of Physics and Astronomy, Univ. of St Andrews, St Andrews, Scotland KY16 9SS, UK*
[5]*ESO, Karl-Schwarzschild-Str. 2, D-85748 Garching, Germany*
[6]*Crimean Astrophysical Observatory, Nauchny 298409, Crimea*
[7]*CFHT Corporation, 65-1238 Mamalahoa Hwy, Kamuela, HI 96743, USA*
[8]*Département de physique, Université de Montréal, C.P. 6128, Succursale Centre-Ville, Montréal, QC H3C 3J7, Canada*
[9]*Institute of Astronomy and Astrophysics, Academia Sinica, PO Box 23-141, 106, Taipei, Taiwan*
[10]*Kavli Institute for Astronomy and Astrophysics, Peking University, Yi He Yuan Lu 5, Haidian Qu, Beijing 100871, China*

ABSTRACT

We present a spectropolarimetric study of the classical T Tauri star (cTTS) LkCa 15 investigating the large-scale magnetic topology of the central star and the way the field connects to the inner regions of the accretion disc. We find that the star hosts a strong poloidal field with a mainly axisymmetric dipole component of 1.35 kG, whereas the mass accretion rate at the surface of the star is $10^{-9.2}$ $M_{\odot}$ yr^{-1}. It implies that the magnetic field of LkCa 15 is able to evacuate the central regions of the disc up to a distance of 0.07 au at which the Keplerian orbital period equals the stellar rotation period. Our results suggest that LkCa 15, like the lower mass cTTS AA Tau, interacts with its disc in a propeller mode, a regime supposedly very efficient at slowing down the rotation of cTTSs hosting strong dipolar fields.

Key words: techniques: polarimetric – stars: formation – stars: imaging – stars: individual: LkCa 15 – stars: magnetic fields.

1 INTRODUCTION

Although major progress was achieved in the last few decades in understanding how low-mass stars and their planets form, many critical phases in this evolution are still poorly understood and are waiting for a consistent physical explanation. The way protostars and their protoplanetary accretion discs succeed at expelling the initial angular momentum and magnetic flux inherited from the parent molecular cloud, before ending up as slowly rotating T Tauri stars with much weaker fields than flux conservation would imply, is one of them. The last step of this process, where the newly formed low-mass stars (called classical T Tauri stars/cTTSs when they still accrete from their discs) interact with the core disc regions through magnetic funnels and apparently succeed at locking their rotation on that of the inner disc, has been the subject of many theoretical and observational studies (Bouvier et al. 2014).

To progress on this issue one critically needs observational constraints on the large-scale fields that control the star–disc interaction

and the loss of angular momentum, and on how these fields relate to the observed diversity of accretion modes that continuous photometric campaigns from space probes like CoRoT or K2 revealed (Cody et al. 2014; Sousa et al. 2016; Cody & Hillenbrand 2018). The main mechanism identified to date as capable of efficiently slowing down the rotation of cTTSs is the magnetic propeller or magnetospheric ejection model (e.g. Romanova et al. 2004; Ustyugova et al. 2006; Zanni & Ferreira 2013), in which the magnetic field of the central star is strong enough to truncate the inner accretion disc at or beyond the corotation radius and efficiently expel angular momentum outwards.

For stellar parameters typical to cTTSs (e.g. 1 $M_{\odot}$, 2 $R_{\odot}$, and a rotation period of 8 d), the dipole component of the large-scale field needs to be stronger than 1–4 kG for accretion rates in the range 10^{-9} to 10^{-8} $M_{\odot}$ yr^{-1} (Bessolaz et al. 2008). However, very few cTTSs are known to host magnetic fields with such strong dipole components; only the prototypical cTTS AA Tau was unambiguously found to be in such a state (Donati et al. 2010), whereas others like V2129 Oph (Donati et al. 2011) may only sporadically reach it. Hence, the need to explore the large-scale fields of a wide sample of cTTSs and unveil the strengths of the dipole component of their

fields, to confirm whether the magnetic propeller is indeed the main process that forces cTTSs into slow rotation.

This can be achieved using phase-resolved spectropolarimetric observations coupled to tomographic imaging techniques inspired from medical imaging (e.g. Donati et al. 2006; Donati & Landstreet 2009). In this paper, we study the well-known cTTS LkCa 15, whose accretion disc, called a transition disc from the fact that it features a wide dust gap from the inner disc up to 50 au from the central star, is reported to be potentially warped (Oh et al. 2016) with claims of ongoing planet formation (Kraus & Ireland 2012; Sallum et al. 2015, later challenged by Thalmann et al. 2015, 2016; Mendigutía et al. 2018). Whereas our paper concentrates on the magnetic field of LkCa 15, a companion study focusses on the properties of its inner accretion disc (Alencar et al. 2018). This companion paper demonstrates in particular that, like AA Tau (Bouvier et al. 2007; Esau, Harries & Bouvier 2014), LkCa 15 is a periodic 'dipper' regularly eclipsed by a dusty inner disc warp connected to accretion funnels and crossing the line of sight as the star rotates, with line profile variations and veiling variability consistent with a highly inclined inner disc interacting with the stellar magnetosphere. Following a short review of the evolutionary status of LkCa 15, we carry out our tomographic imaging study and discuss its implications for our understanding of stellar formation.

2 EVOLUTIONARY STATUS OF LKCA 15

To ensure homogeneity and consistency with previous MaPP and MaTYSSE papers, we start our study with a short revision of the evolutionary status of LkCa 15, incorporating the latest relevant measurements from the literature.

Applying our spectral classification tool (Donati et al. 2012) to our best data (see Section 3), we obtain that the photospheric temperature and logarithmic surface gravity are, respectively, equal to $T_{eff} = 4500 \pm 50$ K and $\log g = 4.0 \pm 0.1$ (in cgs units), in good agreement with results of Alencar et al. (2018). From its measured $B - V$ photometric colour of 1.26 (Grankin et al. 2008) and the one we can expect of a young star of this temperature (1.10 ± 0.02, Pecaut & Mamajek 2013), we obtain a first estimate for the visual extinction of $A_V = 0.68 \pm 0.20$; averaging with the literature value derived from the $V - R_J$ colour ($A_V = 0.41$, Grankin et al. 2008), we adopt a value of $A_V = 0.55 \pm 0.20$. We also obtain a bolometric correction of -0.64 ± 0.02 (Pecaut & Mamajek 2013).

Starting from a maximum V magnitude of 11.87 ± 0.10 (Grankin et al. 2008) and using the latest distance estimate from *Gaia* (158.8 ± 1.3 pc, Gaia Collaboration 2018), we obtain for LkCa 15 a bolometric magnitude of 4.68 ± 0.25, i.e. a logarithmic luminosity relative to the Sun of 0.02 ± 0.10. Comparing with the pre-main sequence evolutionary models of Siess, Dufour & Forestini (2000, assuming solar metallicity and including convective overshooting), we find that LkCa 15 is a $M_\star = 1.25 \pm 0.10$ M$_\odot$ star with a radius of $R_\star = 1.6 \pm 0.2$ R$_\odot$ and an age of $\simeq 5$ Myr. These models further indicate that LkCa 15 is no longer fully but presumably still largely convective, with a convective depth of $\simeq 0.55 R_\star$, and is expected to turn largely radiative (in radius) within less than a few Myr. Compared to our previously studied cTTSs, we note that LkCa 15 is similar to, though slightly less massive and older than, the well-known cTTS V2129 Oph (Donati et al. 2011).

Given the rotation period of LkCa 15 (5.70 ± 0.10 d, Alencar et al. 2018, see also Section 3) and its line-of-sight projected rotation velocity ($v \sin i \simeq 13$ km s^{-1}, see Section 4), we obtain that $R_\star \sin i = 1.46 \pm 0.10$ R$_\odot$, and thus that i, the angle between the rotation axis and the line of sight, ranges between 50° and 90°.

Table 1. Journal of ESPaDOnS observations of LkCa 15. All observations consist of sequences of four subexposures, each lasting 765 s. Columns, respectively, list, for each observation, the UT date, time, Barycentric Julian Date (BJD), peak signal to noise ratio S/N (per 2.6 km s^{-1} velocity bin), rms noise level in Stokes V LSD profiles, and rotation cycle r computed using ephemeris BJD (d) $= 2457343.8 + 5.70r$ as in Alencar et al. (2018).

Date (2015)	UT (hh:mm:ss)	BJD (2 457 340 +)	S/N	σ_{LSD} (0.01%)	r
Nov. 18	12:49:11	5.03967	160	2.8	0.217
Nov. 22	10:24:04	8.93898	180	2.4	0.902
Nov. 23	10:24:13	9.93909	170	2.5	1.077
Nov. 24	08:36:48	10.86452	110	4.2	1.239
Nov. 24	09:32:38	10.90329	150	3.1	1.246
Nov. 25	08:35:51	11.86388	160	2.9	1.415
Nov. 26	08:20:02	12.85291	160	2.7	1.588
Nov. 27	07:51:33	13.83313	160	2.8	1.760
Nov. 28	08:46:46	14.87149	150	2.8	1.942
Nov. 29	10:21:57	15.93760	170	2.6	2.129
Nov. 30	11:53:53	17.00145	160	2.8	2.316
Dec. 01	10:23:42	17.93882	160	2.9	2.481
Dec. 02	12:09:32	19.01233	170	2.6	2.669
Dec. 03	09:01:12	19.88154	180	2.3	2.821

Whereas this remains compatible with the inclination angle of the outer disc ($\simeq 50°$, Thalmann et al. 2014; van der Marel et al. 2015), our tomographic modelling (see Section 4) suggests that i needs to be at least 70° to ensure an optimal fit to the spectropolarimetric data, implying that the inner disc is likely warped as already suggested by previous studies (Oh et al. 2016). This is also supported by the fact that LkCa 15 is a periodic 'dipper' (Alencar et al. 2018), with the inner disc warp regularly occulting the star as it rotates, and requiring i to be within 70–90° (Cody & Hillenbrand 2018).

3 SPECTROPOLARIMETRIC OBSERVATIONS

Our set of observations, carried within the MaTYSSE programme (Donati et al. 2014), consists of 14 circularly polarized spectra collected in late 2015 with the ESPaDOnS spectropolarimeter at Canada–France–Hawaii Telescope (CFHT), covering 370–1000 nm at a resolving power of 65 000 (Donati 2003). Raw frames were reduced with the standard ESPaDOnS reduction package, and least-squares deconvolution (LSD; Donati et al. 1997) was applied to all spectra, using a line list appropriate to LkCa 15. The full journal of observations is presented in Table 1.

A few unpolarized (Stokes I) spectra (at cycles 1.239, 1.588, 1.760, and 1.942) were affected by moonlight in the blue wing of the photospheric lines. This pollution was filtered with the technique we previously devised, which proved efficient and accurate (Donati et al. 2016, 2017b).

Circular polarization (Stokes V) LSD profiles all show clear Zeeman signatures indicating the unambiguous detection of magnetic fields at the surface of LkCa 15, and revealing longitudinal fields (i.e. line-of-sight projected magnetic fields averaged over the visible hemisphere) ranging from −43 to 90 G (see Fig. 1, bottom left panel). Zeeman signals are also clearly detected in the He I D_3 emission line (thought to probe the footpoints of the magnetic funnels linking the surface of cTTSs to their inner accretion discs) as well as in the core emission of the Ca II infrared triplet (IRT) lines (presumably probing both the chromosphere and the accretion regions). The corresponding longitudinal fields reach up to 0.7 and 2 kG for the Ca II IRT and He I lines, respectively, at phases of maximum emission (0.3–0.5, see Fig. 1, middle and bottom right panel for the
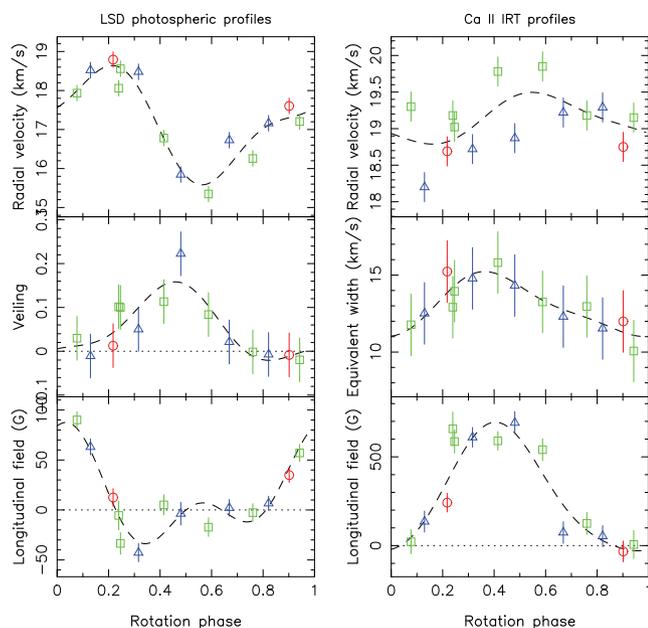
Figure 1. Variability of the LSD profiles (left) and Ca II IRT emission cores (right) of LkCa 15 as a function of rotation phase. Each panel shows the radial velocity (top), the equivalent width (or veiling in the case of LSD profiles, middle), and the longitudinal field (bottom). The red circles, green squares, and blue triangles depict measurements obtained during rotation cycle 0, 1, and 2, respectively, whereas the dashed line shows a sine plus first harmonic fit to the data. Positive longitudinal fields correspond to fields pointing towards the observer.

Ca II IRT lines), with the weaker fields in Ca II IRT lines reflecting the fact that emission from the post-shock accretion region is diluted with chromospheric emission (whereas He I emission suffers little to no dilution from the chromosphere). The mass accretion rate we derive from the maximum emission fluxes in the He I D_3 and Ca II IRT lines is found to be $10^{-9.2 \pm 0.3}$ M$_\odot$ yr^{-1}, in good agreement with Alencar et al. (2018).

Rotational modulation is obvious from LSD photospheric profiles (see Fig. 1, left-hand panel) and yields rotation periods of 5.70 ± 0.06 d, 5.77 ± 0.16 d, and 5.63 ± 0.12 d for the longitudinal field, veiling, and radial velocity (RV), respectively. Modulation is also obvious in Ca II IRT and He I emission (with periods of 5.82 ± 0.16 d and 5.65 ± 0.08 d, respectively) and longitudinal fields from Ca II IRT emission (with period of 5.50 ± 0.15 d). Since all periods we derive are quite consistent (within 1.5σ) with the rotation period used to phase our data (5.70 d, see Table 1), we report no evidence for differential rotation at the surface of LkCa 15.

4 TOMOGRAPHIC MODELLING OF LKCA 15

We use tomographic imaging, and more specifically Zeeman–Doppler Imaging (ZDI), to simultaneously reconstruct the large-scale magnetic field at the surface of LkCa 15, and the distributions of photospheric brightness and accretion-induced excess emission in Ca II IRT lines. To achieve this we proceed as in previous studies (e.g. Donati et al. 2011, 2012) where the imaging method was outlined. We thus only recall the main steps in this paper.

ZDI iteratively looks for a set of images with lowest information content that fits the data at a given reduced chi-square level, starting from blank images containing no information. Whereas photospheric brightness (with cool spots only) and accretion-induced

excess emission (with bright features only) are directly described through their distributions at the surface of the star, the large-scale magnetic field, decomposed into its poloidal and toroidal components, is expressed as a set of spherical harmonics (SH, Donati et al. 2006). We assume the field is dominated by odd SH modes (as in, e.g. Donati et al. 2011) to ensure that accretion occurs mostly towards the polar regions.

The local Stokes I and V profiles of both photospheric lines and Ca II emission are computed using Unno–Rachkovsky's analytical solution to the polarized radiative transfer equations, taking into account the local values of the modelled distributions (i.e. the brightness map for photospheric lines, the accretion map for Ca II emission, and the magnetic map for both sets of lines). Local profiles are then integrated over the visible hemisphere to obtain the synthetic profiles of the rotating star at each observed phase.

Our model is able to convincingly reproduce most observed profile distortions and Zeeman signatures, as shown in Fig. 2. We note that the sharp increase and decrease of the longitudinal field of Ca II IRT lines are better matched for an inclination angle i of 70° than of 50° (the angle measured for the outer accretion disc, Thalmann et al. 2014, with no reliable inclination estimate for the inner disc). We also obtain that the data are best fit for $v \sin i = 12.8 \pm 0.2$ km s^{-1} and for an average radial velocity of LkCa 15 with respect to the Sun of $v_{\rm rad} = 17.4 \pm 0.1$ km s^{-1}.

The reconstructed distributions are shown in Fig. 3. The magnetic map shows a strong radial field region at intermediate latitudes and phase 0.4 where the field strength reaches 2.2 kG, in agreement with the observed longitudinal fields of both Ca II IRT lines (see Fig. 1, bottom right panel) and He I line (see Section 3). This magnetic field region coincides with a large dark photospheric spot, causing longitudinal fields as seen in LSD photospheric profiles to be much weaker than those probed by accretion lines; it also overlaps with a region of excess Ca II emission tracing the footpoints of the magnetic funnel linking the surface of LkCa 15 to the innermost regions of the accretion disc.

We find that the large-scale magnetic field is mostly poloidal, with a poloidal component storing 85 per cent of the magnetic energy. This poloidal component mainly consists of a 1.35 kG dipole tilted at $\simeq 20°$ to the rotation axis (towards phase 0.40) and enclosing $\simeq 75$ per cent of the poloidal field energy; the dipole field strength changes by $\simeq 25$ per cent for a 10° change in the assumed inclination. The poloidal field also includes a -0.9 kG octupole component (i.e. anti-parallel with the main dipole), gathering $\simeq 20$ per cent of the poloidal field energy, and tilted by $\simeq 20°$ to the rotation axis (towards phase 0.95).

5 SUMMARY AND DISCUSSION

We carried out a spectropolarimetric monitoring of the well-known cTTS LkCa 15 with ESPaDOnS at CFHT to detect and model its large-scale magnetic field, and estimate the strength of its dipole component. From a spectroscopic analysis of our data, we first obtain that LkCa 15 is a $\simeq 5$ Myr star with a mass of 1.25 ± 0.10 M$_\odot$ and a radius of 1.6 ± 0.2 R$_\odot$ according to the evolution models of Siess et al. (2000), and thus appears as a slightly older and less massive version of V2129 Oph, another well-studied cTTS (Donati et al. 2011).

Zeeman signatures from LkCa 15 are clearly detected, both in photospheric and accretion lines. Our tomographic study reveals that LkCa 15 hosts a strong and mostly poloidal large-scale field, reaching up to 2.2 kG at the surface of the star, with a dipole component of 1.35 kG. Given the accretion rate at the surface of
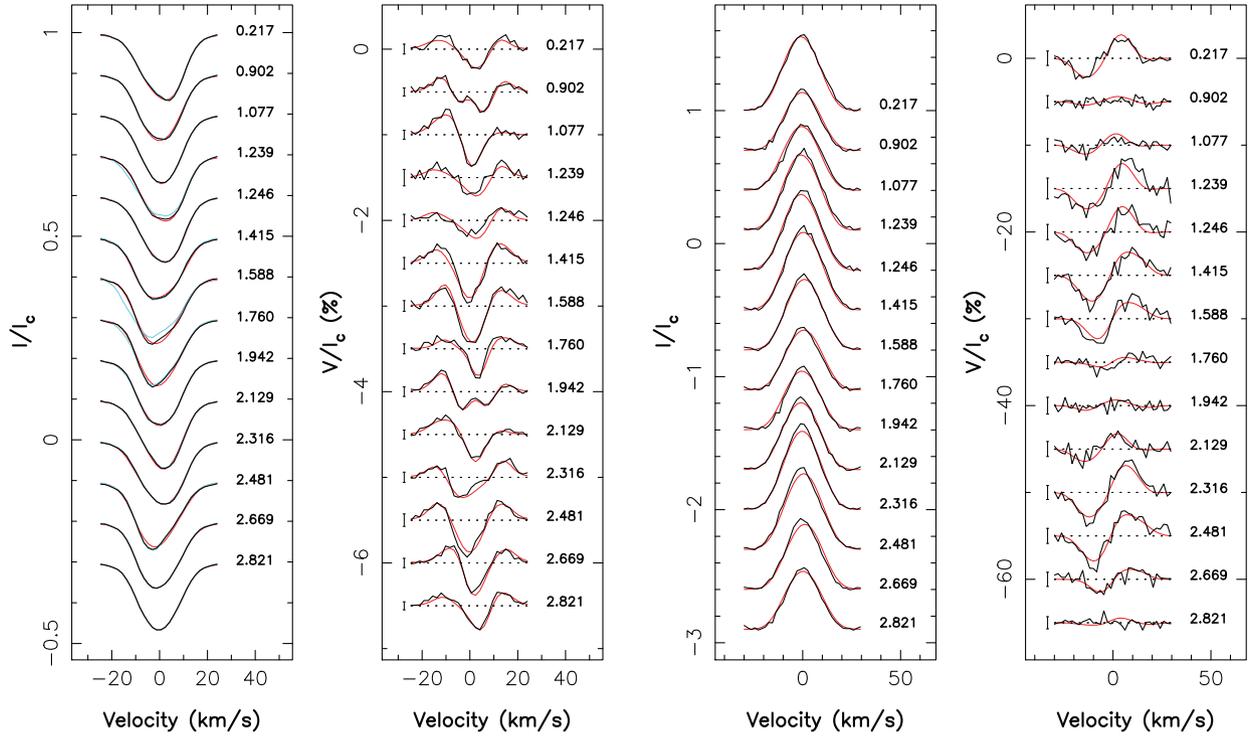
Figure 2. Observed (thick black line) and modelled (thin red line) LSD Stokes *I* and *V* profiles of the photospheric lines (lef-handt panels) and of the emission core of IRT lines (right-hand panels) of LkCa 15. Rotation cycles and 3σ error bars (for Stokes *V* profiles only) are indicated right and left to each observation, respectively. LSD Stokes *I* photospheric profiles before correcting from moon pollution (at cycles 1.239, 1.588, 1.760, and 1.942) are shown in cyan (leftmost panel).
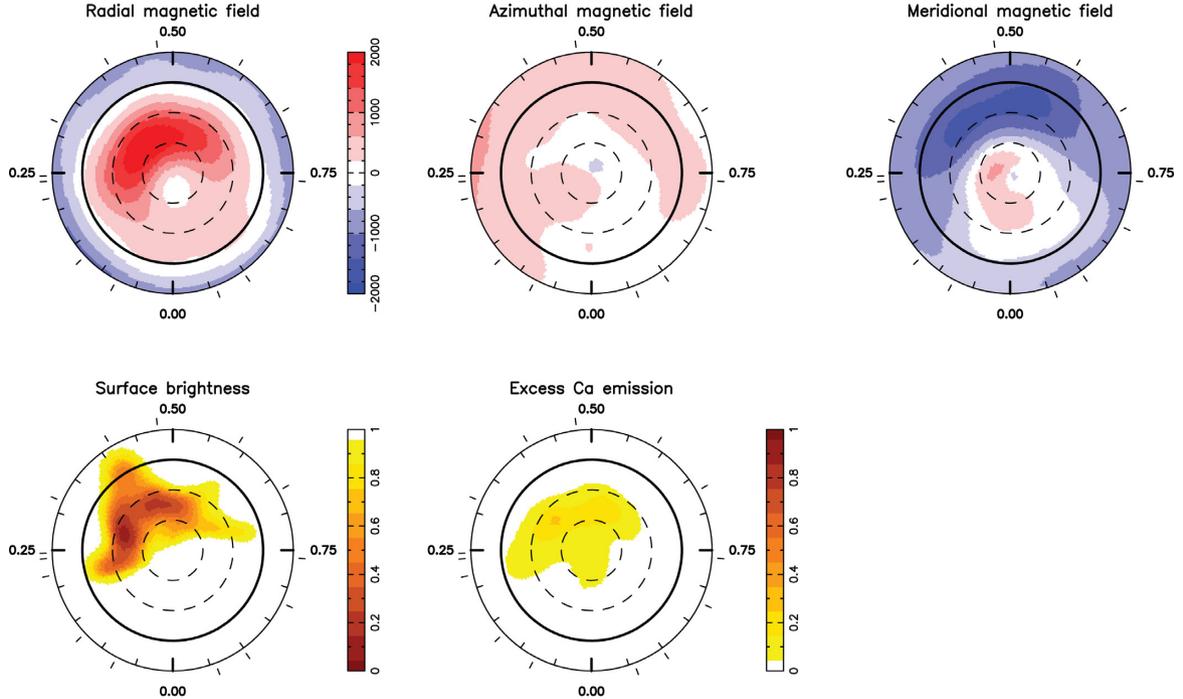

Figure 3. Reconstructed maps of the magnetic field (top left, middle, and right panels for the radial, azimuthal, and meridional components in spherical coordinates, all in G), relative photospheric brightness (bottom left), and excess accretion-induced Ca II core emission (bottom right) at the surface of LkCa 15, derived from the data set of Fig. 2 using tomographic imaging. The star is shown in a flattened polar projection down to a latitude of $-30°$, with the north pole at the centre and the equator shown as a bold line. Outer ticks depict phases of observations. Positive radial, azimuthal, and meridional fields, respectively, point outwards, counter clockwise, and polewards.

the star, found to be equal to $10^{-9.2}$ M$_\odot$ yr^{-1} from emission fluxes in the He I and Ca II IRT lines (see Section 3), we can conclude from Bessolaz et al. (2008) that the magnetospheric cavity that the field carves at the disc centre reaches out to the corotation radius, located at a distance of 0.07 au. Our result suggests that LkCa 15 is in a propeller accretion regime, capable of counteracting the natural angular acceleration of the contracting star. In fact, LkCa 15 is a good match to the C01 simulation of Zanni & Ferreira (2013), where the spin-down torque from the star–disc coupling is found to dominate the spin-up torque from both the accreted material and the contracting star. Besides, photometric monitoring tells that accretion at the surface of LkCa 15 is unsteady (Alencar et al. 2018, as for AA Tau), agreeing again with predictions from simulations (Zanni & Ferreira 2013). This is also consistent with recent studies concluding that LkCa 15 triggers outflows from the inner disc (Fang et al. 2018; Mendigutía et al. 2018).

Given that LkCa 15 is already close to 50 per cent convective in radius (see Section 2), we can speculate that the dipole component of its large-scale field is likely to be strongly reduced as the star contracts and becomes mostly radiative (Donati & Landstreet 2009; Gregory et al. 2012; Donati et al. 2013). As a result, LkCa 15 is likely to start speeding up towards the main sequence in a few Myr. Simulations are needed to investigate in a more documented and quantitative way the rotational history of cTTSs like LkCa 15 under the combined effect of irregular accretion and evolving large-scale fields.

We stress the importance of studying the large-scale fields of a wide sample of cTTSs like LkCa 15 to better understand the physics of star–disc interactions, and more generally its impact on early stellar evolution. Studying how magnetic fields relate to the various types of magnetospheric accretion revealed through continuous photometry (Cody et al. 2014; Sousa et al. 2016; Cody & Hillenbrand 2018) seems particularly promising in this respect. New generation spectropolarimeters working in the nIR like SPIRou (Donati et al. 2017a), giving access to even younger and lower mass stars and offering an enhanced sensitivity to magnetic fields, should be a prime asset for this task.

REFERENCES

Alencar S. et al., 2018, A&A, https://arxiv.org/abs/1811.04806
Bessolaz N., Zanni C., Ferreira J., Keppens R., Bouvier J., 2008, A&A, 478, 155
Bouvier J. et al., 2007, A&A, 463, 1017
Bouvier J., Matt S. P., Mohanty S., Scholz A., Stassun K. G., Zanni C., 2014, Protostars and Planets VI. Univ. of Arizona, Tucson, p. 433
Cody A. M., Hillenbrand L. A., 2018, AJ, 156, 71
Cody A. M. et al., 2014, AJ, 147, 82
Donati J., Landstreet J. D., 2009, ARA&A, 47, 333
Donati J. et al., 2010, MNRAS, 402, 1426
Donati J. et al., 2011, MNRAS, 412, 2454
Donati J.-F., 2003, in Trujillo-Bueno J., Sanchez Almeida J., eds, ASP Conf. Ser. Vol. 307. *Solar Polarization*. Astron. Soc. Pac., San Francisco, p. 41
Donati J.-F., Semel M., Carter B. D., Rees D. E., Collier Cameron A., 1997, MNRAS, 291, 658
Donati J.-F. et al., 2006, MNRAS, 370, 629
Donati J.-F. et al., 2012, MNRAS, 425, 2948
Donati J.-F. et al., 2013, MNRAS, 436, 881
Donati J.-F. et al., 2014, MNRAS, 444, 3220
Donati J. F. et al., 2016, Nature, 534, 662
Donati J.-F. et al. 2017a, in Deeg H. J., Belmonte J. A., eds, Handbook of Exoplanets, Springer Nature, Switzerland, p. 107
Donati J.-F. et al., 2017b, MNRAS, 465, 3343
Esau C. F., Harries T. J., Bouvier J., 2014, MNRAS, 443, 1022
Fang M. et al., 2018, *ApJ*, in press (preprint arXiv:1810.03366)
Gaia Collaboration, 2018, A&A, 616, A1
Grankin K. N., Bouvier J., Herbst W., Melnikov S. Y., 2008, A&A, 479, 827
Gregory S. G., Donati J.-F., Morin J., Hussain G. A. J., Mayne N. J., Hillenbrand L. A., Jardine M., 2012, ApJ, 755, 97
Kraus A. L., Ireland M. J., 2012, ApJ, 745, 5
Mendigutía I., Oudmaijer R. D., Schneider P. C., Huélamo N., Baines D., Brittain S. D., Aberasturi M., 2018, A&A, 618, L9
Oh D. et al., 2016, PASJ, 68, L3
Pecaut M. J., Mamajek E. E., 2013, ApJS, 208, 9
Romanova M. M., Ustyugova G. V., Koldoba A. V., Lovelace R. V. E., 2004, ApJ, 616, L151
Sallum S. et al., 2015, Nature, 527, 342
Siess L., Dufour E., Forestini M., 2000, A&A, 358, 593
Sousa A. P. et al., 2016, A&A, 586, A47
Thalmann C. et al., 2014, A&A, 566, A51
Thalmann C. et al., 2015, ApJ, 808, L41
Thalmann C. et al., 2016, ApJ, 828, L17
Ustyugova G. V., Koldoba A. V., Romanova M. M., Lovelace R. V. E., 2006, ApJ, 646, 304
van der Marel N., van Dishoeck E. F., Bruderer S., Pérez L., Isella A., 2015, A&A, 579, A106
Zanni C., Ferreira J., 2013, A&A, 550, A99

This paper has been typeset from a TEX/LATEX file prepared by the author.